Journal of
Applied Crystallography
ISSN 0021-8898
Editor: **Anke R. Kaysser-Pyzalla**

Low-Σ twist and tilt grain boundaries in cubic materials

A. Morawiec

J. Appl. Cryst. (2011). **44**, 1152–1156

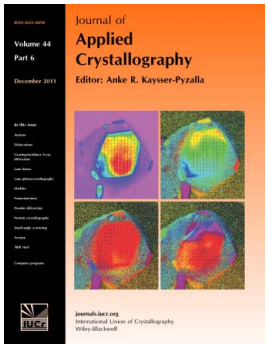

Journal of
Applied Crystallography
ISSN 0021-8898

Received 24 August 2011
Accepted 18 October 2011

Low-Σ twist and tilt grain boundaries in cubic materials

A. Morawiec

Polish Academy of Sciences, Institute of Metallurgy and Materials Science, Reymonta 25, 30–059 Kraków, Poland. Correspondence e-mail: nmmorawi@cyf-kr.edu.pl

Knowledge of the geometry of grain boundaries in polycrystalline materials is essential for predicting boundary properties. The issue of cataloging the geometrically characterized groups of twist and tilt boundaries is addressed. All distinct types of pure-twist and pure-tilt boundaries are determined for misorientations corresponding to highly coincident ($3 \leq \Sigma \leq 13$) lattices of cubic symmetry. For these particular misorientations, the number of distinct twist boundaries and zones of tilt boundaries ranges from 5 ($\Sigma = 3$) to 11 ($\Sigma = 9$ or 11). Maps displaying the locations of twist and tilt boundary planes indicate boundaries having particular geometries with two-dimensional periodicities. This is of significance for identification of special boundary structures. Moreover, the maps allow for relating peaks on experimentally determined grain boundary distributions to particular types of twist or tilt boundaries.

1. Introduction

A grain boundary network is an important component of a polycrystalline aggregate (see *e.g.* Sutton & Balluffi, 1995). Although boundary geometry is not sufficient for predicting boundary properties, knowing and understanding the geometry is a prerequisite for more complete boundary analyses. An experimentally accessible paradigm of the boundary geometry involves macroscopic boundary parameters: the grain misorientation and the boundary plane (Goux, 1974). Among various types of boundaries that can be distinguished on the basis of the macroscopic parameters are those known as twist boundaries and tilt boundaries. Definitions of twist and tilt boundaries involve the axis of the misorientation and the boundary plane, and – what needs to be emphasized – they take into account crystal symmetry; because of the symmetry, a boundary can be represented in numerous ways, and only some of these representations may explicitly reveal its special geometric features. A twist boundary is a boundary having a representation with the misorientation axis perpendicular to the boundary plane, and a tilt boundary has a representation with the axis in the boundary plane.

Twist and tilt boundaries usually appear in case studies of bicrystals. In polycrystalline research, a statistical approach is more suitable, and the interest is not in individual boundaries but in boundary types. Therefore, it is important to classify the boundaries. The issue of making an inventory of twist and tilt boundaries, to our knowledge, has not been considered before. It is justified to focus on boundaries with misorientations corresponding to coincident site lattices (CSLs) (Kronberg & Wilson, 1949). This paper catalogs all twist and tilt boundaries between crystallites of cubic $m\bar{3}m$ symmetry for low-Σ CSL misorientations (up to Σ13; here and below, the '=' sign is omitted for brevity). The twist and tilt boundaries are also presented in two-dimensional maps of varying boundary planes for fixed misorientations. Similar figures have been extensively used for displaying distributions of boundaries over the space of boundary parameters (see *e.g.* Rohrer *et al.*, 2010, and references therein). These experimentally determined distributions depict frequencies of occurrence of particular boundary types in investigated polycrystals. Conclusions concerning the occurrence of twist and tilt boundaries have been drawn from such distributions on a number of occasions, *e.g.* by Rohrer *et al.* (2004, 2010) and Randle *et al.* (2008), but – with symmetries ignored – many twist and tilt boundaries have been overlooked. As we show below, the complete set of twist and tilt boundaries is larger than that considered in reference to boundary distributions. The maps showing where all these boundaries are located facilitate the task of correctly ascribing peaks of intensity in boundary distributions to twist or tilt boundaries. At the end of this article, we discuss a link between specific boundary geometries and boundary structures. These limited considerations are carried out at the scale of macroscopic parameters in relation to the presented catalog and maps. Throughout the paper, the conventions of Morawiec (2009*b*) are used.

2. Locations of twist and tilt boundary planes for a fixed misorientation

Five-parameter grain boundary distributions are conveniently displayed in two-dimensional sections with fixed misorientations and variable boundary planes. Since the plane of a twist boundary is perpendicular to the misorientation axis, such planes are determined by the misorientation parameters. Therefore, in the sections corresponding to fixed misorienta-

tions, twist boundaries are represented by isolated poles or points. If a tolerance is added, the points take the form of spots. Tilt boundaries are limited only by the perpendicularity of the misorientation axis and the normal to the boundary plane. Therefore, in the sections with fixed misorientations, tilt boundaries are represented by lines (or bands, if a tolerance is added; see Fig. 1). The goal here is to determine all twist and tilt boundaries for low-Σ misorientations, *i.e.* to find the locations of poles of twist and tilt boundary planes in the sections corresponding to these misorientations.

We begin with considering twist boundaries. Let us focus on the $\Sigma3$ misorientation obtained by 60° rotation about the [111] axis. It is clear that, with this misorientation, the boundary in the (111) plane is a twist boundary. Let us now consider the plane $(3\bar{1}1)$. This plane is not perpendicular to the misorientation axis, and it is not obvious that it also has the twist character. To see this, one needs to consider symmetrically equivalent representations of this boundary. It turns out (see Appendix *A*) that application of a crystal symmetry operation to one of the crystals gives a representation in which the plane indices are $(31\bar{1})$ and $(\bar{3}\bar{1}1)$ for the first and second crystals, respectively, and the misorientation corresponds to a rotation about $[\bar{3}\bar{1}1]$. In this representation, the misorientation axis is perpendicular to the boundary plane, so indeed the considered boundary is a twist boundary.

By systematically proceeding in analogous fashion with other planes, one obtains all twist boundaries for the selected $\Sigma3$ misorientation. In reality, our software calculated a suitably defined (Morawiec, 2009*b*,*c*) distance to the nearest pure-twist boundaries for a grid of points in the domain of boundary planes. The density of the grid was 1° in polar coordinates of normals to the planes. The pure-twist boundary nearest to a given boundary of the grid was calculated *via* function minimization using the *MINUIT* package (James, 1998) and a procedure analogous to that described by Morawiec (2009*c*). Points of the grid characterized by very small distances to pure-twist boundaries reveal the positions of the latter. The thus obtained locations of twist boundary planes are shown as the first pole figure of Fig. 2. The figure exhibits symmetries because the [111] misorientation axis is a symmetry axis of the crystal. Consequently, some spots

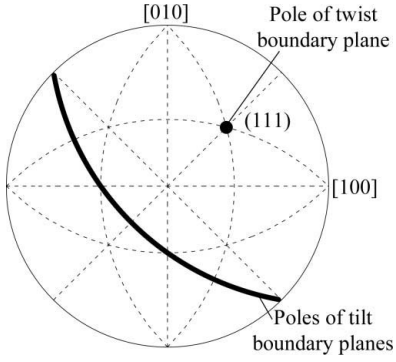

Figure 1
Stereographic projection of the (111) pole and the poles of the [111] zone. Assuming the ([111], 60°) misorientation, (111) is the plane of a twist boundary, and the planes of the [111] zone are tilt-boundary planes.

Table 1
Parameters of the investigated misorientations: misorientation axis (*a*) and misorientation angle (*b*).

Σ	*a*	*b* (°)
3	[111]	60.000
5	[100]	36.870
7	[111]	38.213
9	[110]	38.942
11	[110]	50.479
13*a*	[100]	22.620
13*b*	[111]	27.796
39	[123]	50.132

represent equivalent boundaries. It turns out that there are exactly five macroscopically distinct $\Sigma3$ twist boundaries.

A similar approach was applied to other low-Σ CSL misorientations. Parameters of the investigated misorientations are given in Table 1. Maps of twist boundaries for these misorientations are shown in Fig. 2. For $\Sigma5$, 7, 9, 11, 13*a* and 13*b*, there are, respectively, 7, 8, 11, 11, 7 and 8 macroscopically distinct types of twist boundaries. Their representatives are listed in Table 2.

As for the tilt boundaries, their planes are arranged into zones, *i.e.* sets of planes parallel to one axis. In the considered case of cubic symmetry, the zones are directly linked to planes of twist boundaries. For a fixed misorientation, a given rotation axis of a twist boundary is a zone axis of planes of tilt boundaries, and conversely, a zone axis of planes of tilt boundaries is also an axis of a twist boundary (see Fig. 1). Thus, Table 2, which lists the Miller indices of twist boundary planes (and numerically equal indices of twist axes), concurrently gives the indices of the zone axes of tilt boundaries. Accordingly, in the maps shown in Fig. 2, there is a one-to-one correspondence of the zone axes of tilt boundaries and the poles of twist boundary planes. Analogously to the case of twist boundaries, the maps of tilt boundaries were determined by calculating the distance to the nearest pure-tilt boundaries for each point of the grid in the domain of boundary planes.

Since the rotation axes of the considered CSL misorientations happen to be symmetry axes, the distributions of spots and bands in the pole figures of Fig. 2 are adequately symmetric. For comparison, example nonsymmetric distributions for a high-Σ misorientation are shown in Fig. 3.

Our method of determining twist and tilt boundaries and of generating data for Fig. 2 was purely numerical. [This approach was used because a part of the needed software already existed; we employed routines written for use in previous work (Morawiec, 2009*c*).] However, the same results can be obtained by a combination of analytical considerations and more effective numerical calculations. A boundary is described as twist or tilt based on the position of the misorientation axis with respect to the boundary plane. In the cubic case, there are up to 24×24 distinct misorientation axes corresponding to distinct rotations representing a given physical misorientation. Each of the permissible misorientation axes may correspond to a twist boundary plane and a zone of tilt boundary planes, and these boundaries can be obtained from a list of the axes. By application of the symmetry

operations, one obtains equivalent representations of the misorientation and, hence, the list of permissible misorientation axes. Then, one needs to loop over the axes of the list, and to verify whether the boundary based on the initial misorientation and the boundary plane perpendicular to a given axis of the list is a twist boundary; if so, the axis also determines a zone of tilt boundaries. The verification requires the checking of all equivalent representations of the boundary (as in the example given in Appendix *A*).

3. Twist–tilt boundaries and multiple tilt boundaries

As expected, for low-Σ CSL misorientations, the planes of twist boundaries (and thus the axes of zones of tilt boundary planes) have low Miller indices. Most of them are of the type {*hk*0} and {*hkk*} (with analogous indices for the zone axes). Of the 57 distinct types listed in Table 2, only six are different. It is clear that, for low-Σ misorientations, most twist boundaries are also tilt boundaries (*cf.* Fortes, 1973). There are two distinct twist non-tilt boundaries each for Σ9 and Σ11. As noted by Morawiec (2009*a*), the lowest Σ for which a twist boundary cannot be a tilt boundary is 39; the corresponding maps are shown in Fig. 3.

It is sensible to ask about the significance of differences among boundaries exposed in Figs. 2 and 3. Are there any

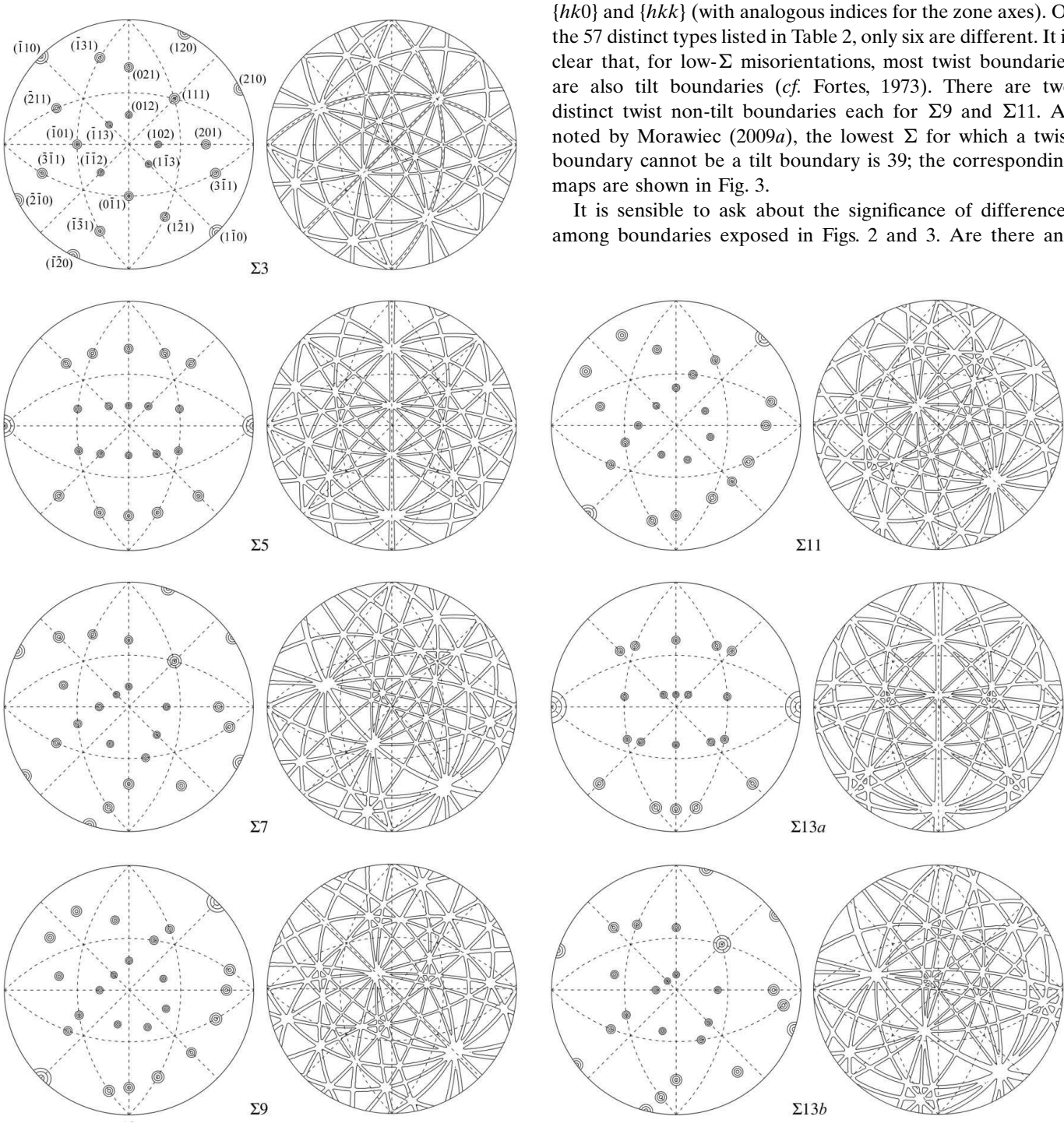

Figure 2
Locations of poles of twist (the left-hand map of each pair) and tilt (right-hand maps) boundary planes for low-Σ CSL misorientations. Different spot sizes and band widths are an artefact of the used software; the lines represent distances from pure-twist (1, 2 and 3° isolines) or pure-tilt (0.8° isoline) boundaries.

Table 2
List of distinct twist boundaries and zones of tilt boundaries for low-Σ CSL misorientations.

The table is arranged as follows. For a given misorientation (Σ), the first column (*a*) contains the Miller indices of the plane of a twist boundary (and thus, numerically equal indices of the zone axis of the tilt boundaries) in the particular representation of the misorientation Σ as listed in Table 1. The following two columns contain the axis (*b*), say [*uvw*], and the angle (*c*) of an equivalent misorientation in which the boundaries have explicitly twist or tilt character. In this equivalent representation, the planes of the twist boundary are $(\bar{u}\,\bar{v}\,\bar{w})$ and (*uvw*) in the reference frames of the first and second crystal, respectively. For instance, for Σ3 ([111], 60° misorientation), the plane $(3\bar{1}1)$ corresponds to a twist boundary, and $[3\bar{1}1]$ is a zone axis of tilt boundaries. The initial ([111], 60°) misorientation is equivalent to ($[\bar{3}\bar{1}1]$, 146.443°). In this equivalent representation, the plane of the twist boundary is $(31\bar{1})$ (first crystal) and $(\bar{3}\bar{1}1)$ (second crystal). If a given twist boundary is also a tilt boundary, the multiplicity of tilt is listed in the last column (*d*).

	a	*b*	*c* (°)	*d*
Σ3	(1 1 1)	$[\bar{1}\,\bar{1}\,\bar{1}]$	60.000	6
	$(1\bar{2}1)$	$[\bar{2}\,1\,1]$	180.000	6
	$(1\bar{1}0)$	$[\bar{1}\,0\,1]$	70.529	2
	(2 0 1)	[2 1 0]	131.810	1
	$(3\bar{1}1)$	$[\bar{3}\,1\,1]$	146.443	1
Σ5	(1 0 0)	[1 0 0]	36.870	4
	(0 2 1)	$[0\,\bar{2}\,\bar{1}]$	180.000	6
	(1 2 1)	[1 2 1]	101.537	1
	(2 2 1)	$[2\,\bar{1}\,2]$	143.130	1
	(0 1 3)	$[\bar{1}\,0\,\bar{3}]$	180.000	6
	(1 1 3)	$[1\,\bar{1}\,3]$	95.739	1
	(3 1 3)	$[3\,\bar{1}\,3]$	154.158	1
Σ7	(1 1 1)	[1 1 1]	38.213	3
	$(\bar{1}\,\bar{2}\,3)$	$[1\,\bar{3}\,\bar{2}]$	180.000	7
	$(2\bar{1}0)$	[2 0 1]	73.398	1
	$(5\bar{1}1)$	$[1\,1\,\bar{5}]$	158.213	1
	(3 0 1)	[3 1 0]	115.377	1
	(0 3 2)	$[0\,\bar{2}\,\bar{3}]$	148.997	1
	$(\bar{1}\,2\,1)$	$[1\,\bar{2}\,1]$	135.585	1
	$(\bar{3}\,3\,1)$	$[3\,1\,\bar{3}]$	110.925	1
Σ9	(1 1 0)	$[\bar{1}\,1\,0]$	38.942	2
	(3 1 5)	[5 3 1]	160.812	
	$(\bar{2}\,3\,1)$	$[\bar{3}\,1\,\bar{2}]$	123.749	
	(5 1 1)	$[\bar{1}\,5\,\bar{1}]$	120.000	1
	(4 0 1)	$[\bar{4}\,0\,1]$	152.734	1
	$(3\bar{1}1)$	$[\bar{3}\,1\,1]$	67.115	1
	$(2\bar{2}1)$	$[\bar{2}\,\bar{2}\,1]$	180.000	8
	(2 3 2)	$[\bar{2}\,3\,\bar{2}]$	152.734	1
	(1 2 2)	$[1\,\bar{2}\,\bar{2}]$	90.000	2
	(0 1 2)	[2 1 0]	96.379	1
	$(\bar{1}\,1\,4)$	$[\bar{4}\,1\,1]$	180.000	8
Σ11	(1 1 0)	[1 1 0]	50.479	2
	$(3\bar{1}5)$	$[1\,5\,\bar{3}]$	126.222	
	(2 1 4)	$[\bar{4}\,1\,\bar{2}]$	155.380	
	(4 1 1)	$[4\,1\,\bar{1}]$	129.521	1
	(3 0 1)	$[\bar{3}\,0\,1]$	144.903	1
	$(2\bar{1}1)$	$[\bar{1}\,2\,\bar{1}]$	62.964	1
	$(3\bar{3}2)$	$[\bar{3}\,\bar{3}\,\bar{2}]$	180.000	8
	(3 5 3)	$[\bar{5}\,\bar{3}\,3]$	162.659	1
	(1 3 3)	$[1\,\bar{3}\,\bar{3}]$	82.163	2
	(0 2 3)	[2 0 3]	100.476	1
	$(\bar{1}\,1\,3)$	$[\bar{1}\,1\,\bar{3}]$	180.000	8
Σ13*a*	(1 0 0)	[1 0 0]	22.620	4
	(0 3 2)	$[\bar{2}\,3\,0]$	180.000	6
	(2 3 2)	$[2\,\bar{3}\,2]$	107.920	1
	(3 3 2)	$[\bar{3}\,\bar{3}\,2]$	133.813	1
	(0 1 5)	$[\bar{1}\,0\,\bar{5}]$	180.000	6
	(1 1 5)	$[5\,\bar{1}\,\bar{1}]$	92.204	1
	(5 1 5)	[5 5 1]	164.058	1
Σ13*b*	(1 1 1)	[1 1 1]	27.796	3
	$(\bar{1}\,\bar{3}4)$	$[\bar{3}\,4\,\bar{1}]$	180.000	7
	$(3\bar{1}0)$	$[\bar{3}\,0\,1]$	76.658	1
	$(7\bar{1}1)$	$[\bar{7}\,1\,1]$	164.058	1
	(4 0 1)	[4 1 0]	107.920	1
	(0 4 3)	$[3\,0\,\bar{4}]$	157.380	1
	$(\bar{3}\,5\,3)$	$[5\,\bar{3}\,3]$	130.832	1
	$(\bar{2}\,2\,1)$	$[\bar{2}\,1\,\bar{2}]$	112.620	1

indications for some boundaries to be more 'special' than other boundaries? The most prominent interface among high-angle boundaries is the coherent twin boundary (Σ3 misorientation, {111} plane) of materials with the A1 structure. In low and moderate stacking fault energy metals, this boundary has special properties. What makes the coherent twin boundary different is the boundary plane corresponding to high coincidence of atom positions at the boundary. As can be seen in Fig. 2, the twin boundary [Σ3, (111)] not only is a twist boundary but can also be obtained by tilts about the $[1\bar{1}0]$, $[01\bar{1}]$, $[\bar{1}01]$, $[\bar{2}11]$, $[\bar{1}\,\bar{1}2]$ and $[1\bar{2}1]$ directions. Thus, it is natural to look for other high-angle boundaries of similar type, *i.e.* with a twist axis and multiple tilt axes. Such boundaries can be easily identified in Fig. 2. They correspond to spots (of twists) intersected by multiple bands (of tilts). The multiplicities of the intersections for particular twist boundaries are listed in the last column of Table 2. The highest multiplicity tilts are the well known 180° twists (Haüy's twins by hemitropy) about low-index axes. However, as the pole figures of Fig. 2 demonstrate, these twins do not exhaust the list of boundaries with elevated (>1) multiplicities of tilts; *e.g.* [Σ3, $(1\bar{1}0)$] has the multiplicity of 2. It is also worth noting that some boundaries satisfy the condition of high multiplicity approximately; an example boundary of this kind is marked in Fig. 3.

For simple crystal structures like A1 and A2 with atomic sites only at lattice nodes, the particular geometries of boundaries having multiple-tilt character are directly linked to

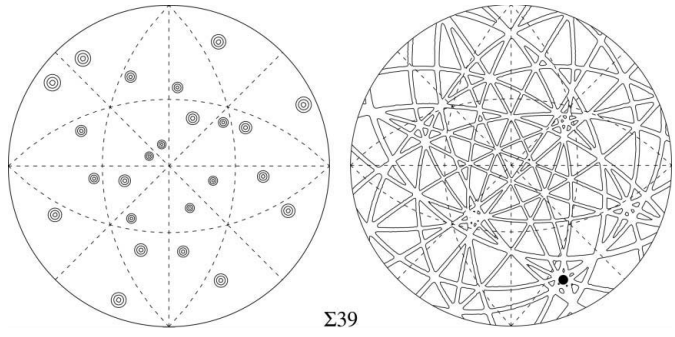

Figure 3
Locations of twist and tilt boundaries for the Σ39 misorientation with the parameters given in Table 1. The figures are nonsymmetric; there are 24 distinct twist boundary types and 24 distinct zones of tilt boundaries, and there are no boundaries having both twist and tilt character. The disc marks the $(5\,\bar{1}\,\bar{1}\,3)$ plane of a twist boundary; it does not have exact tilt character but it deviates only slightly from numerous zones of tilt boundaries. Isolines as in Fig. 2.

boundary structures. Boundaries with multiple tilt axes are periodic along multiple nonparallel directions in the boundary plane, *i.e.* they are two-dimensionally periodic. If these periodicities happen to be along low-index directions, the periods are relatively short and the repeat cell is small. With higher (than average) ordering at such boundaries, special boundary properties can be expected.

4. Conclusions

This paper provides a list of all possible twist boundaries and zones of tilt boundaries for low-Σ CSL misorientations in the case of $m\bar{3}m$ crystal symmetry. The boundaries are also drawn in two-dimensional maps analogous to those displaying experimental grain boundary distributions. The maps can be used for estimating the actual frequencies of occurrence of particular twist or tilt boundaries in experimentally investigated materials.

It is clear from the maps that some low-Σ CSL boundaries exhibit simple geometries. Particularly interesting are two-dimensionally periodic boundaries with multiple tilt axes; many of them have also the twist character. Their simple geometries may correspond to specific structures and, consequently, to special physical properties of boundaries.

Our considerations were limited to a particular crystal symmetry and, for the sake of space, to only a few misorientations. Clearly, one can proceed in the same way with other misorientations, and it becomes feasible to index all twist and tilt boundaries in the cubic case. Moreover, similar procedures can be applied to other crystal symmetries with a center of inversion.

It is expected that this article will contribute to a better understanding of geometry of grain boundaries and also to improved interpretation of experimental grain boundary distributions.

APPENDIX *A*
Equivalent boundary representations

We consider the boundary corresponding to a 60° rotation about [111] ($\Sigma 3$ misorientation) with the $(3\bar{1}1)$ plane in the first crystallite. In the notation of Morawiec (2009*b*), this boundary is represented by the matrix

$$\mathbf{B} = \frac{1}{3}\left(\begin{array}{c|ccc} 0 & -3a & -1a & 1a \\ \hline 3a & 2 & 2 & -1 \\ -1a & -1 & 2 & 2 \\ 1a & 2 & -1 & 2 \end{array}\right), \qquad (1)$$

where $a = 3/11^{1/2}$ is the normalization coefficient, the 3×3 matrix is the orthogonal matrix of the misorientation, and the first column (row) contains normalized indices of the plane in the coordinate system of the first (second) crystallite. By application of all crystal symmetry operations, one obtains different representations of the same boundary. Let us focus on one of these operations, namely on the half-turn of the first crystal about the [100] axis. The explicit form of the symmetry operator is

$$\mathbf{C} = \left(\begin{array}{c|ccc} 1 & 0 & 0 & 0 \\ \hline 0 & 1 & 0 & 0 \\ 0 & 0 & -1 & 0 \\ 0 & 0 & 0 & -1 \end{array}\right), \qquad (2)$$

and the application of the operation corresponds to multiplication of **C** and **B**,

$$\mathbf{CB} = \frac{1}{3}\left(\begin{array}{c|ccc} 0 & -3a & -1a & 1a \\ \hline 3a & 2 & 2 & -1 \\ 1a & 1 & -2 & -2 \\ -1a & -2 & 1 & -2 \end{array}\right). \qquad (3)$$

In this new representation, the planes have indices $(31\bar{1})$ and $(\bar{3}\bar{1}1)$ for the first and the second crystal, respectively, and the misorientation corresponds to the 146.4° rotation about the $[\bar{3}\bar{1}1]$ axis, *i.e.* the misorientation axis is perpendicular to the boundary plane.

References

Fortes, M. A. (1973). *Acta Cryst.* A**29**, 68–70.
Goux, C. (1974). *Can. Metall. Quart.* **13**, 9–31.
James, F. (1998). *MINUIT. Function Minimization and Error Analysis, Reference Manual*. Version 94.1. http://wwwasdoc.web.cern.ch/wwwasdoc/minuit/minmain.html.
Kronberg, M. L. & Wilson, F. H. (1949). *Trans. AIME*, **185**, 501–514.
Morawiec, A. (2009*a*). *J. Appl. Cryst.* **42**, 308–311.
Morawiec, A. (2009*b*). *J. Appl. Cryst.* **42**, 783–792.
Morawiec, A. (2009*c*). *Scr. Mater.* **61**, 438–440.
Randle, V., Rohrer, G. S., Miller, H. M., Coleman, M. & Owen, G. T. (2008). *Acta Mater.* **56**, 2363–2373.
Rohrer, G. S., Li, J., Lee, S., Rollett, A. D., Groeber, M. & Uchic, M. D. (2010). *Mater. Sci. Technol.* **26**, 661–669.
Rohrer, G. S., Saylor, D. M., El-Dasher, B., Adams, B. L., Rollett, A. D. & Wynblatt, P. (2004). *Z. Metallkd.* **95**, 197–214.
Sutton, A. P. & Balluffi, R. W. (1995). *Interfaces in Crystalline Materials*. Oxford: Clarendon Press.